IOPscience iopscience.iop.org

Home Search Collections Journals About Contact us My IOPscience

Graphene nanotransistors for RF charge detection

This content has been downloaded from IOPscience. Please scroll down to see the full text.

2014 J. Phys. D: Appl. Phys. 47 094004

(http://iopscience.iop.org/0022-3727/47/9/094004)

View the table of contents for this issue, or go to the journal homepage for more

Download details:

IP Address: 129.199.117.151
This content was downloaded on 12/02/2014 at 13:59

Please note that terms and conditions apply.

IOP Publishing Journal of Physics D: Applied Physics
J. Phys. D: Appl. Phys. 47 (2014) 094004 (5pp) doi:10.1088/0022-3727/47/9/094004

Graphene nanotransistors for RF charge detection

E Pallecchi[1,2], Q Wilmart[1], A C Betz[1,3], S-H Jhang[1,4], G Fève[1], J-M Berroir[1], S Lepillet[2], G Dambrine[2], H Happy[2] and B Plaçais[1]

[1] Laboratoire Pierre Aigrain, Ecole Normale Supérieure, CNRS (UMR 8551), Université P. et M. Curie, Université D. Diderot, 24, rue Lhomond, 75231 Paris Cedex 05, France
[2] Institut d'Electronique, de Microélectronique et de Nanotechnologie, UMR-CNRS 8520, BP 60069, Avenue Poincaré, 59652, Villeneuve d'Asq, France

E-mail: Bernard.Placais@lpa.ens.fr

Received 6 May 2013, revised 13 September 2013
Accepted for publication 23 September 2013
Published 12 February 2014

Abstract
We have studied the static and dynamical properties of a graphene microwave nanotransistor to be used as sensitive fast charge detectors. The channel consists of exfoliated graphene on SiO_2 with a 120 nm long, 900–1500 nm wide top-gate deposited on 5 nm AlO_x dielectric. The scattering parameters were measured up to 60 GHz from which we deduce the gate capacitance, the drain conductance and the transconductance as a function of gate voltage. The broad measuring band allows us to measure the current gain and to map its full spectrum so as to extract reliable values of the transit frequency f_T. From these measurements, we could estimate the carrier mobility, the doping of the access leads, the gate capacitance and the transconductance. The transconductance per unit width and bias voltage is larger than 1 mS μm^{-1} V^{-1} which compares with the performance of high electron mobility transistors. High-frequency characterization is achieved using microwave probe stations. Finally, using recent noise thermometry measurements, we estimate the charge resolution of graphene nanotransistors.

(Some figures may appear in colour only in the online journal)

1. Introduction

Graphene is a high mobility material. This property stems from the material quality, as well as intrinsic factors such as the suppression of backscattering by chirality and the very weak phonon scattering. The latter is, on the other hand, also responsible for large electronic temperatures due to poor phonon cooling of carriers. Mobilities in excess of $\mu = 10^5$ cm^2 V^{-1} s^{-1}, initially obtained with suspended graphene, are now reproduced in graphene supported on hexagonal boron nitride (h-BN) substrates which opens the route to ballistic microwave graphene electronics [1]. This requires additionally the integration of well coupled top and/or bottom gates. At room temperature the mobility still exceeds that of semiconductors by two orders of magnitude thanks to a large optical phonon energy. This favours more classical microwave electronics including radio-frequency (RF) transistors. These have been extensively studied using CVD graphene on diamond [2] and epitaxial graphene on SiC [2, 3] or exfoliated graphene on h-BN [4]. They show large transit frequencies f_T's (the current gain cutoff) up to 350 GHz at the shortest gate length $L_g \lesssim 40$ nm [2]. A figure of merit is the product $f_T L_g$ which peaks at 15 GHz μm. Similar values have been reported with exfoliated graphene on sapphire [5] or bilayer graphene on h-BN [6] with, however, a better score for bottom gated graphene on h-BN devices with $f_T L_g \simeq 24$ GHz μm [4]. They correspond to saturation velocities $V_{sat} \sim 10^5$ m s^{-1}, which are one order of magnitude below expectations based on the Fermi velocity $v_F = 10^6$ m s^{-1}. There are several explanations for this limitation; the leading one is a saturation of f_T due to emission of surface polar phonons (SPPs) of the substrate and/or dielectrics that have an energy that is generally below the optical phonons energy of graphene (∼160 meV) [7]. A similar

[3] Present address: Hitachi Cambridge Laboratory, JJ Thomson Avenue, CB23 0HE Cambridge, UK.
[4] Present address: Department of Physics, Konkuk Uinversity, 120 Neungdong-ro, Gwangjin-gu, Seoul 143-701, Korea.

 © 2014 IOP Publishing Ltd Printed in the UK

effect is observed for plasmon life time in infrared optics [8]. Although there is room for technological optimization to enhance f_T's, a more severe limitation of classical graphene RF transistors is the small voltage gain, due to the semi-metallic character of graphene. This corresponds to a low power gain cutoffs $f_{MAX}/f_T \lesssim 1$ in graphene [4, 3] as compared with semiconducting transistors where $f_{MAX}/f_T \gtrsim 1$.

In this work we consider an application that does not rely on f_{MAX} at all. It consists of graphene nano-field-effect transistors (nanofet), with a typical gate width $W \lesssim 1\,\mu$m, to be used as fast charge/current converter. At cryogenic temperature, graphene nanofet can potentially allow for the on-the-flight single electron detection at GHz frequency. The conversion factor, which determines the charge sensitivity, is simply f_T irrespective of the voltage gain (or f_{MAX}). Of course these converters should be followed by a low-noise power amplifier stage to preserve the high resolution. The charge resolution of a graphene nanofet $q^* = \sqrt{S_I}/(2\pi f_T)$ is then controlled by the current noise S_I and the transit frequency $f_T = g_m/2\pi C_g$, where g_m and C_g are the transconductance and gate capacitance. As $g_m \propto C_g \propto W$ and $S_I \propto I_{ds} \propto W$ one has $q^* \propto \sqrt{W}$ which qualifies nanofets with small channel width as fast and sensitive charge detectors. The ultimate miniaturization can be reached using single carbon nanotube RF transistors [9, 10], for which an intrinsic charge resolution of $q^* = 13\,\mu e/\sqrt{\text{Hz}}$ has been estimated. This promising sensitivity is, however, hampered by the large impedance mismatch of the device and the following amplification stage.

The mismatch is much smaller in graphene-based nanofets, where the channel resistance is typically one to two orders of magnitude smaller than for nanotube FETs. To evaluate the nanofet charge sensitivity, dealing with biased conductors, we estimate the noise using the Johnson–Nyquist formula $S_I = 4g_{ds}k_B T_e$, where g_{ds} is the channel conductance and T_e the electronic temperature. In carbon-based conductors, T_e is mostly controlled by cooling processes which involve the emission of acoustic phonons (below 1000 K). In graphene, the exact cooling power depends on lattice temperature and doping [11, 12], with laws that differ from those of carbon nanotubes [13]. In this work we have realized graphene nanofets (W = 900–1500 nm) using exfoliated graphene on SiO_2 and measured their microwave properties up to 60 GHz. We have also used a simple model to analyse data and estimate the resolution of graphene nanotransistor charge detectors.

2. Experimental principles

Graphene nanotransistors were fabricated using exfoliated graphene flakes deposited onto a high resistivity thermally oxidized silicon substrate. Graphene flakes were identified by the analysis of the optical contrast, and micro-Raman spectroscopy was used to verify their mono-layer nature. We first defined the source and drain electrodes using e-beam lithography with a PMMA resist. In order to minimize the contact resistance, 40 nm of palladium were used as contact material. In a second lithography step, a 50 Ω matched coplanar waveguide was defined and realized by metallization of Ti/Au 5/100 nm. The gate oxide was then prepared by evaporating 2 nm of aluminum, which was oxidized by exposing the sample to air. We estimate by AFM the gate oxide thickness $t = 5 \pm 1$ nm. Aluminum oxide has been extensively employed as gate oxide in graphene microwave devices [14]. The quality of our oxide is sufficient for demonstration of graphene in charge sensing, where the issue of reproducibility is less critical than in commercial RF transistors. Typical breakdown voltage of our oxide is on the order of 2.5 V, leak current is smaller than 1 nA at 1 V. For better performances, AlO_x could be replaced by 5 nm thick hexagonal boron nitride, since this material is known to help increasing the graphene mobility, and it suppresses both hysteresis and leak current. Finally, we patterned the top-gate electrode, followed by evaporation of a Ti/Au bilayer (5/100 nm). The contact spacing, which defines the transistor channel length, was chosen at 300 nm, while the gate length was 120 nm. The batch consisted of 10 devices processed on the same wafer, from their dc characteristics we selected the best 5 which we have characterized at microwave frequencies. In this experiment no dummy structures, i.e. identical device ghost structures that are devoid of graphene were included. The channel width, defined by the width of the graphene flakes, varies from 900 to 1500 nm. A micrograph of a finished sample is shown in figure 1. Our design differs from the symmetric double gated design typically used for RF transistors. The reason behind this choice lies in our ultimate goal of an on-the-fly detection of single electrons, which requires a single gate transistor. Microwave measurements were carried out in a variable temperature 60 GHz microwave probe station. The scattering parameters (S-parameters) were measured and converted into admittance parameters (Y-parameters) for direct comparison with the small-signal equivalent circuit of figure 1(*c*). In the absence of dummy structures, we could not subtract the extrinsic stray capacitance contributions, C_{gs0}, C_{ds0} and C_{gd0} (see in figure 1(*c*)), which contribute additively to the Y-matrix. The dc characteristics were measured simultaneously.

3. Experimental results and analysis

Figure 2 shows a subset of dc characteristics for sample $S1$ ($W = 1.2\,\mu$m) which were measured at 77 K. The gate voltage values are indicated in the inset. The current shows a weak sub-linear behaviour above 100 mV indicative of the good mobility of the sample. The drain–source resistance (inset) shows a p-type doping and an ON/OFF ratio of ∼2.5. The low value of the ON/OFF ratio, which originates from the absence of bandgap in graphene, is not critical for charge sensing applications, as is the case considered in our work. Higher ON/OFF can be obtained by considering graphene bilayer or vertical transistors [15, 16].

The extrinsic Y-parameters, measured for $V_{ds} = 200$ mV and frequencies up to 60 GHz and temperatures down to 77 K, are displayed in figure 3. Taking $Y_{11} \simeq Y_{gs}$ we estimate the gate capacitance which is dominated by the extrinsic term $C_{gs0} \simeq \Im(Y_{11})/\omega \simeq 32$ fF. Similarly, using $Y_{22} \simeq Y_{ds}$, we deduce $C_{gd0} \simeq C_{gs0}$ (not shown) and the RF drain–source conductance, $g_{ds} \simeq \Re(Y_{22})$. g_{ds} shows a significant gate dependence, similar to that measured at dc,

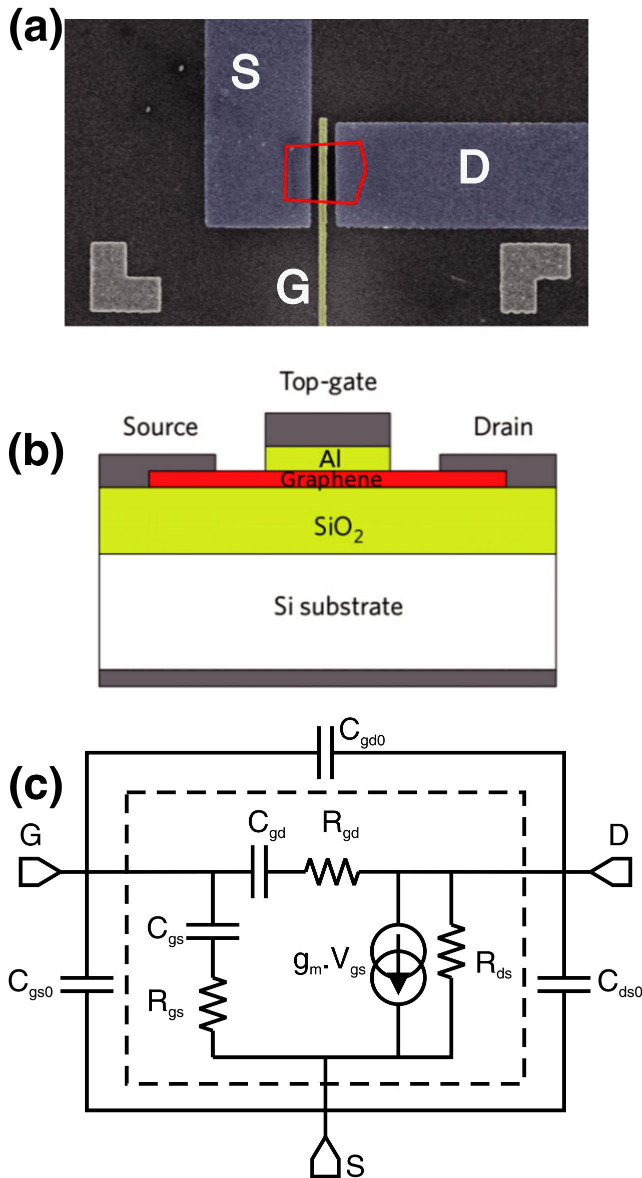

Figure 1. (a) Scanning electron micrograph of a typical graphene nanotransistor, where graphene flake contours are highlighted in red. The gate length, 120 nm, sets the scale of the figure. (b) schematic cross-section of the nanofet. (c) Small-signal equivalent circuit of the graphene nanotransistor used for scattering parameter analysis. Extrinsic components are displayed outside the dashed rectangle. Notations are explained in the text.

that has no obvious frequency dependence. We also observe an additive contribution $\propto \omega^2$ which is not accounted for by the model (possibly a shorting of the contact resistance by capacitive coupling). The oscillations above 50 GHz are due to calibration imperfections. The gate–drain admittance, $Y_{gd} \simeq Y_{21}$, is characteristic of graphene RF capacitor [14]. We deduce $C_{gd}+C_{gd0} \simeq 2.6$ fF and $R_{gd} \simeq 400\ \Omega$. The comparison with (half) the geometrical capacitance $C_{geo}/2 \simeq 0.8$ fF, points towards a significant extrinsic contribution $C_{gd0} \lesssim 1.8$ fF. In the absence of dummy structure, we could not measure independently C_{gd0}; however, we do obtain $C_{gd0} \ll C_{gs0}$ as expected from geometry.

Finally, we deduce the RF transconductance from $g_m \simeq \Re(Y_{21})$. Its variations as a function of gate voltage

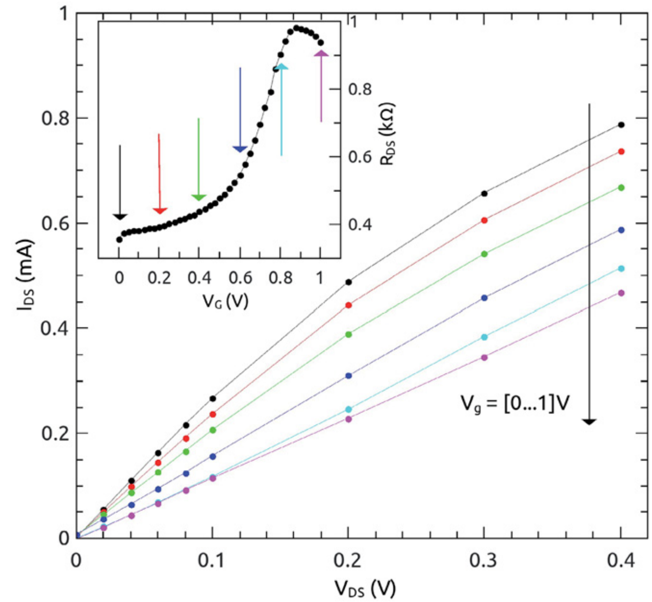

Figure 2. Dc characteristics of sample $S1$ ($W = 1.2\ \mu$m) measured at 77 K. Main panel: the I–V characteristic is controlled by the gate voltage and shows a weak saturation at high bias. Inset: gate voltage dependence of the linear drain–source resistance.

are frequency independent and reach $g_m \simeq 0.35$ mS. The transconductance per micrometre and bias voltage reaches $1.5\ \text{mS}\ \mu\text{m}^{-1}\ \text{V}^{-1}$ which slightly exceeds GaN-HEMT (high electron mobility transistor) standards ($\lesssim 1\ \text{mS}\ \mu\text{m}^{-1}\ \text{V}^{-1}$ [17]) and competes with InAs standards ($\lesssim 4\ \text{mS}\ \mu\text{m}^{-1}\ \text{V}^{-1}$ [18]). The maximum voltage gain $A_V = g_m/g_{ds} \simeq 0.2$ remains modest due to the small channel resistance $R_{ds} \simeq 700\ \Omega$. Figure 5 shows the gate voltage dependence of the transconductance for both positive and negative bias. Note the shift of the transconductance peaks at positive bias.

In order to characterize in more detail the dynamical properties of the transistor we plot in figure 4 the ratio $H_{21}^* = Y_{21}/2Y_{12}$ which is an estimate of the intrinsic current gain $H_{21} = (Y_{21} - jC_{gd0}\omega)/(Y_{11} - jC_{gs0}\omega)$. The factor 2 in the denominator of H_{21}^* relies on the assumption that $C_{gs} \simeq C_{gd}$ by device symmetry. As we cannot subtract the extrinsic term C_{gd0} from Y_{12} due to the absence of de-embedding, we obtain here an underestimate. The current gain shows a characteristic $1/f$-dependence and a saturation at $H_{21} = 1/2$. Thanks to our broadband measurement we cover the full spectrum of the current gain including the high-frequency plateau. The inset of the figure shows the transit frequency, defined as the $H_{21}^* = 1$ intercept, as a function of bias voltage. A saturation is observed at $f_T = 17$ GHz above $V_{ds} \gtrsim 0.2$ V. It corresponds to an underestimate of the saturation velocity $V_{sat} = 2\pi f_T L_g = 13\ \text{GHz}\ \mu\text{m}$. If we now consider that we have underestimated H_{21}, and if we assume that $C_{gd} \sim C_{gd0}/2$, we can estimate the intrinsic transit frequency and saturation velocity at a 2-times larger level. Of course this speculation needs to be confirmed by further measurements, including more accurate de-embedding.

Finally, we can account for the dc and RF properties of our graphene nanofet quite accurately using a simple Drude model of transport in the graphene channel. We use the following

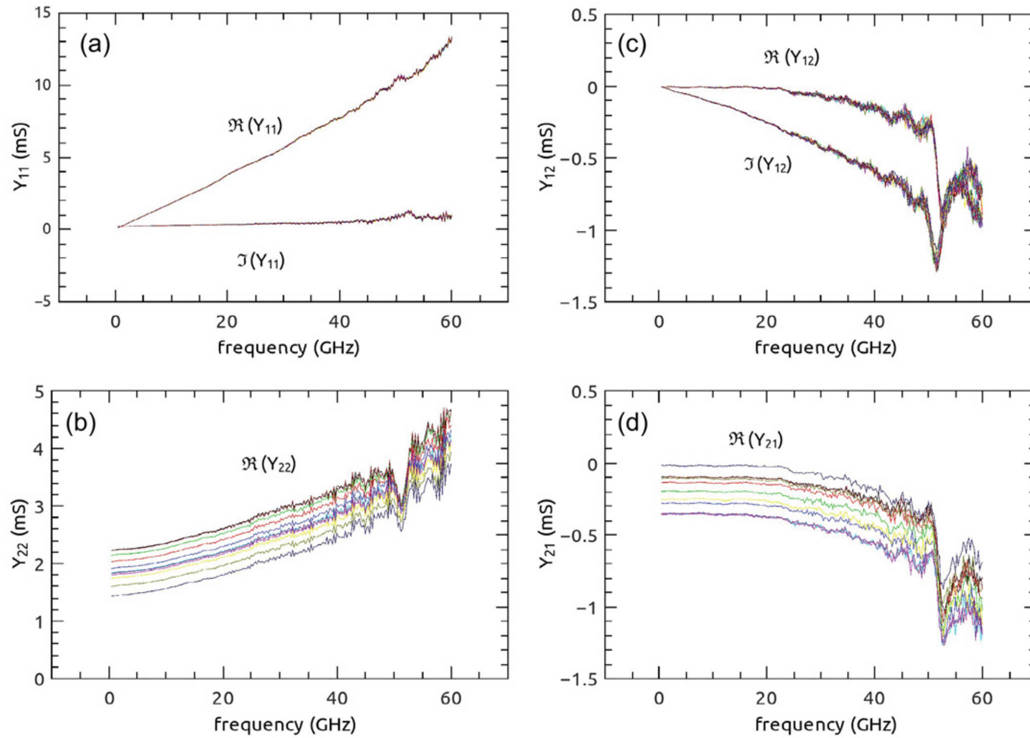

Figure 3. Admittance matrix (Y-parameters) of sample $S1$ measures at 77 K, at 200 mV bias, over the full set of gate voltages specified in figure 2. (a) shows the real and imaginary parts of $Y_{11} \simeq Y_{gs}$ which is dominated by extrinsic contribution $C_{gs0} \simeq 32$ fF. (b) shows the real part of the output admittance $\Re(Y_{22}) \simeq g_{ds}$. ($c$) shows the gate–drain admittance which contains both intrinsic and the parasitic contributions of same order of magnitude. Finally, (d) shows the active contribution of the transistor, i.e. the transconductance $g_m \simeq \Re(Y_{21})$.

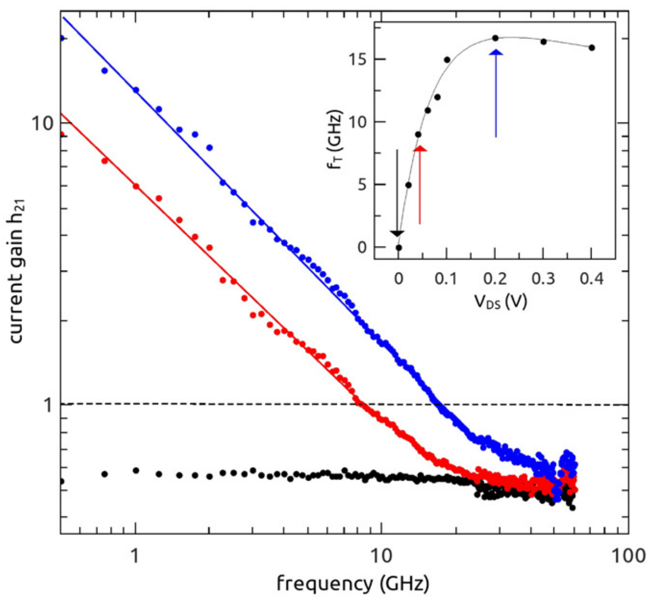

Figure 4. Main panel: spectrum of the current gain of sample $S1$ for bias values specified by colour arrows in the inset. It shows the crossover, at the transit frequency f_T, from the active response ($1/f$ dependence) to the passive response ($H_{21} = 1/2$) at high frequency. The latter corresponds to an equal splitting of the gate current to drain and source. The inset shows the bias dependence of f_T that saturates above 200 mV.

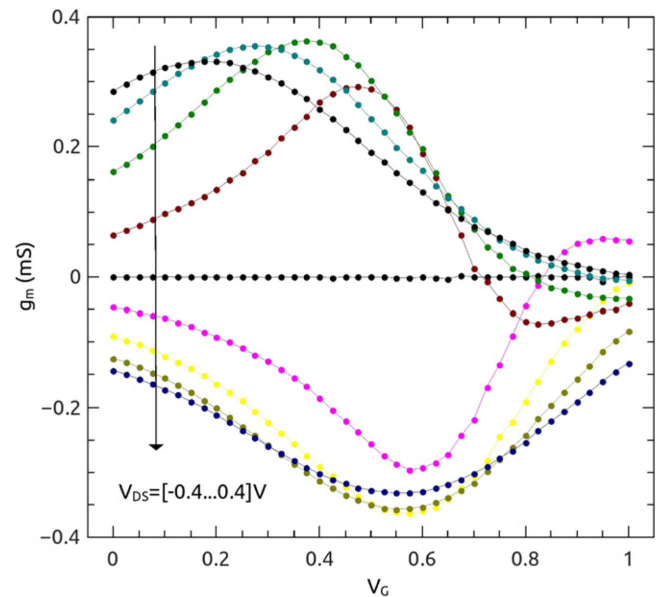

Figure 5. Transconductance of sample $S1$ as a function of gate voltage for positive and negative bias (see the arrows). As seen in the figure, the transconductance starts to saturate above 100 mV. In increasing negative bias the transconductance maximum shifts towards negative gate voltages.

parameters: a contact resistance of 100 Ω µm, an access doping of 4×10^{12} cm^{-2}, a mobility of 1000 cm^2 V^{-1} s^{-1}, $C_{gd0} \lesssim 1.8$ fF, the AlO_x thickness of 5 nm (with a permittivity of 6). Note that the model is constrained as we have five free parameters for six measurable quantities: g_m, g_{ds}, the g_{ON}/g_{OFF} ratio, the gate–drain capacitance, the gate voltage at the working point and in the ON-state (notwithstanding the R_{gd} data). Such a model will prove useful for further optimization of dynamical properties, in particular that of the

intrinsic f_T which is highly relevant for the optimization of graphene nanofet charge detectors.

Finally, we can take advantage of the recent progress in the understanding of carrier cooling pathways in graphene [11, 12] to estimate the electronic temperature T_e in the nanofet channel. Considering cryogenic conditions to secure cold lattice conditions, phonons are kept below the Bloch–Gruneisen temperature and we have $T_e \simeq (P/\Sigma)^{1/4}$ where $P = V_{ds}I_{ds}/WL_g$ is the Joule power per unit area and $\Sigma \sim 1\,\mathrm{mW\,m^{-2}\,K^{-4}}$ the acoustic–phonon coupling constant. Taking these numbers we can estimate $T_e \simeq 500\,\mathrm{K}$ (at $V_{ds} = 200\,\mathrm{mV}$). We can also estimate the charge resolution $q^* = \sqrt{S_I}/(2\pi f_T) \simeq 180\,\mu\mathrm{e}/\sqrt{\mathrm{Hz}}$[5] for our nanofet charge detector. On the one hand, this value is two orders of magnitude larger than that achieved in single electron transistors (SETs) which work in 100 MHz narrow bandwidth [19]. On the other hand, the resolution is one order of magnitude better than that of quantum point contact transistors [20], which work at GHz frequencies. Graphene nanofets are both sensitive and robust up to microwave frequencies. Their present resolution can still be improved to fill the gap with SETs by increasing the mobility (factor 10) and decreasing the channel width (factor 4). This would pave the way to picosecond single charge detectors which are needed in quantum single electronics.

In conclusion, we have demonstrated microwave operation of sub-micrometre graphene transistors (nanofets). We have assessed their performance as sub-nanosecond broadband charge detectors using simple and well established transport and noise models.

Acknowledgments

The research has been supported by the Cnano contracts 'GraFet-e', 'Topin's and Grav's', the ANR-2010-MIGRAQUEL. The work of Q Wilmart is supported by the DGA.

References

[1] Dean C R *et al* 2010 *Nature Nanotechnol.* **5** 725
[2] Wu Y *et al* 2012 *Nano Lett.* **12** 3062
[3] Guo Z *et al* 2013 *Nano Lett.* **13** 942
[4] Meric I, Dean C R, Han S J, Wang L, Jenkins K A, Hone J and Shepard K L 2011 *IEEE Int. Electron Devices Meeting (Washington, DC)*
[5] Pallecchi E, Benz C, Betz A C, von Löhneisen H, Plaçais B and Danneau R 2011 *Appl. Phys. Lett.* **99** 113502
[6] Wang H, Taychatanapat T, Hsu A, Watanabe K, Taniguchi T, Jarillo-Herrero P and Palacios T 2011 *IEEE Electron Device Lett.* **32** 1209
[7] Low T, Perebeinos V, Kim R, Freitag M and Avouris P 2012 *Phys. Rev.* B **86** 045413
[8] Yan H, Low T, Zhu W, Wu Y, Freitag M, Li X, Guinea F, Avouris P and Xia F 2013 *Nature Photon.* **7** 394
[9] Chaste J, Lechner L, Morfin P, Fève G, Kontos T, Berroir J-M, Glattli D C, Happy H, Hakonen P and Plaçais B 2008 *Nano Lett.* **8** 525
[10] Chaste J, Pallecchi E, Morfin P, Fève G, Kontos T, Berroir J-M, Hakonen P and Plaçais B 2010 *Appl. Phys. Lett.* **96** 192103
[11] Betz A C *et al* 2012 *Phys. Rev. Lett.* **109** 056805
[12] Betz A C, Jhang S-H, Pallecchi E, Ferreira R, Fève G, Berroir J-M and Plaçais B 2013 *Nature Phys.* **9** 109
[13] Wu F, Virtanen P, Andresen S, Plaçais B and Hakonen P 2010 *Appl. Phys. Lett.* **97** 262115
[14] Pallecchi E, Betz A C, Chaste J, Fève G, Huard B, Kontos T, Berroir J-M and Plaçais B 2011 *Phys. Rev.* B **83** 125408
[15] Szafranek B N, Schall D, Otto M, Neumaier D and Kurz H 2011 *Nano Lett.* **11** 2640
[16] Britnell L *et al* 2012 *Science* **335** 6071
[17] Nidhi, Dasgupta S, Lu J, Speck J and Mishra U K 2012 *IEEE Electron Device Lett.* **33** 794
[18] Kim D-H *et al* 2012 *Appl. Phys. Lett.* **101** 223507
[19] Andresen S E S, Wu F, Danneau R, Gunnarsson D and Hakonen P J 2008 *J. Appl. Phys* **104** 033715
[20] Gustavsson S, Leturcq R, Simovic B, Schleser R, Ihn T, Studerus P, Ensslin K, Driscoll D C and Gossard A C 2006 *Phys. Rev. Lett.* **96** 076605

[5] The charge sensitivity $\mathrm{d}q$ is easily calculated imposing the change in the bias current $\mathrm{d}I_{bias} = g_m \mathrm{d}V_g = g_m \mathrm{d}q/\mathrm{d}V_g$ equal to the current noise $\mathrm{d}I_{noise} = \sqrt{S_I}$ times bandwidth.